



Stability analysis of a typical landslide mass in the Three Gorges Reservoir under varying reservoir water levels

Yonggang Zhang¹ · Zhen Zhang¹ · Shuai Xue² · Ruijie Wang⁴ · Mao Xiao³

Received: 19 August 2018 / Accepted: 10 December 2019 / Published online: 2 January 2020
© Springer-Verlag GmbH Germany, part of Springer Nature 2020

Abstract

Water level change upstream of a reservoir highlights the risk of a landslide-prone area on the banks of a reservoir. This paper conducted a study on the deformation mechanism of a selected landslide that occurred in the Three Gorges Reservoir (TGR) after the water level of the reservoir changed. The long-monitored surface deformation of the slide mass revealed that the deformation of the landslide was related to the water level changes in the reservoir, especially of the change between flood and floodless seasons. The measured internal lateral displacements in the landslide showed that such a landslide was characterized by a trail-mode. FLAC^{3D} was adopted to model the landslide by examining the plastic zone, factor of safety, and the displacement in the x -direction in consideration of four conditions: the natural state of a landslide in the TGR, the initial impoundment, the subsequent rise of water level, and the drawdown of water level. The numerical results indicated that the landslide mass tended to be unstable during the initial impoundment; the subsequent rise of water level had a limited effect on the landslide happening, but the drawdown of water level directly triggered the landslide. The landslide changed from push-mode to trail-mode. It is strongly recommended that drawdown of the water level in the reservoir be carefully controlled to mitigate the effect on landslide mass.

Keywords Three Gorges Reservoir · Landslide failure · Water level change · Field monitoring · Numerical analysis

List of symbols

- f_s Stress of a certain point in the soil
 σ_1 Maximum principal stress
 σ_3 Minimum principal stress
 φ Internal friction angle
 c Cohesion
 σ_t Tensile strength of soil

Introduction

The Three Gorges Project (TGP) on the Yangtze River, containing the Three Gorges Dam (TGD) located in Hubei Province, is the world's largest hydroelectric project and is regarded as the pivotal project for the impoundment of the TGR (Chai et al. 2009). TGP, which was completed in 2009, controls 1 million km² of drainage area, and is able to store 39.3 billion m³ of water (Deng et al. 2000). Even though the reservoir significantly mitigates the flood damage in this region, the fluctuation of its water level increases the risk of geological hazards (He et al. 2008; Du et al. 2013). The water level in the TGR region was lifted from an elevation of 70 m above sea level to 175 m after the TGD was complete. The water level was lifted to the terminal elevation in three stages: (1) the water level reached an elevation of 135 m on 10 June, 2003, after the TGR started to receive water on 1 June, 2003; (2) the water level reached 156 m by September, 2006; (3) the water level reached 175 m in 2009 after the TGP was complete (Luo et al. 2009).

Water level change upstream of the reservoir highlights the risk of geological hazards on the banks of the reservoir. It is reported that landslide risk has become one of the

✉ Zhen Zhang
dyzhangzhen@gmail.com

¹ Key Laboratory of Geotechnical and Underground Engineering of Ministry of Education, Department of Geotechnical Engineering, Tongji University, Shanghai 200092, China

² Imperial College London, London SW7 2AZ, UK

³ School of Mines, China University of Mining and Technology, Xuzhou 221116, China

⁴ State Key Laboratory of Traction Power, Southwest Jiaotong University, Chengdu 610000, China

primary geological hazards in the reservoir area of the TGR (Yin and Peng 2007; Wang et al. 2008; Zhang et al. 2010; Huang et al. 2012; Xu et al. 2018; Chen et al. 2019; Yu 2019; Bao et al. 2019). Therefore, it is crucial to investigate the failure mechanism of landslides in the TGR area so as to assess the stability of landslide mass and/or take feasible reinforcement measures.

In the past, a number of studies have been conducted to study the deformation and failure mechanism of landslide mass, via numerical analysis (Fredlund and Rahardjo 1993; Tinti et al. 1999; Zaniboni and Tinti 2014), field investigation (Keefer et al. 1987; Chelli et al. 2006; Matsuura et al. 2013; Singh et al. 2016) and/or field monitoring (Bovis 1990; Picarelli et al. 2000; Petley et al. 2002; Mayoraz and Vulliet 2002; Sassa et al. 2009; Nguyen et al. 2017; Zhang et al. 2019). However, the influence of water level change on stability of landslide mass has not been clearly addressed. For example, the evolution of plastic zone in landslide body under the influence of water level fluctuation needs to be further studied.

In the present paper, a typical landslide on the bank upstream of TGR reservoir was selected, which occurred after the impoundment of the TGR in 2003. Based on the long field measurement, the deformation characteristics of the landslide with the water level changes were explored. Accordingly, three-dimensional (3-D) analysis using FLAC^{3D} was conducted to investigate the failure mechanism of landslide mass with the fluctuation of water level. Four cases were considered: the natural state of a landslide in the TGR, the initial impoundment, the subsequent rise of water level, and the drawdown of water level.

Geological conditions of the landslide mass

The landslide chosen for this case study is located on the left bank of the Yangtze River, in Wushan County, Hubei Province (Fig. 1). The planar shape of the landslide mass was proximate to a square with a length about 600 m and a width about 500 m (Fig. 2). The contact zone had an average thickness of approximately 2 m. The landslide occupied a mass with an area about $30 \times 10^4 \text{ m}^2$ and a volume about $1500 \times 10^4 \text{ m}^3$. The landslide mass slid along a direction of 150° , nearly perpendicular to the Yangtze River. The elevations of the landslide changed from 135 to 355 m, indicating that the landslide had a maximum vertical elevation difference of 220 m and an average slope angle of 30° . The left and right sides of the landslide mass were bounded by gullies, the trailing edge was bounded by a scarp, the middle part and the trailing edge were steep, and movement along the leading edge of the landslide mass was relatively slow. The landslide mass comprised two areas, defined as blocks A

and B due to the difference in susceptibility to deformation (Fig. 2): the deformation within block A was more significant than that in block B.

The landslide mass was loose, consisting of colluvial and residual silty clay, which was yellow–brown and easily softened by water. The material also contains about 35% rubble, which reduces from the surface to the bottom of the landslide mass, and consists of gray-green silty siltstone of size 5–10 cm.

The sliding surface was the interface between the loose accreted body and the underlying bedrock, which had length of about 600 m, width of about 500 m, dip angle of 30° , and dip direction of 150° . The sliding surface was of ‘linear’ shape, and the middle part of the landslide mass was of ‘convex’ shape. The thickness of the contact zone was about 2 m, mainly comprising clay with a small amount of debris.

The bedrock mainly consisted of silty siltstone, gray-green marlite, and a small amount of magenta mudstone of the Badong Formation in the Triassic. Generally, the upper strata were loose materials, while the lower strata were hard materials. The bedrock was easily weathered due to its low strength, and it was also prone to softening when moistened. The dip direction of the bedrock stratum was 290° , which was opposite to the dip direction of the landslide (Fig. 3). Such stratum distribution resulted in a frequently happening landslide in the area of the TGR.

Field measurement of the landslide

Surface displacement

The deformation of the landslide mass has been observed since the water level of the TGR reached 135 m in 2003. Figure 4 shows the photos taken on the landslide mass. In 2003, tensile cracks along the trailing edge, and numerous cracks on roads built on the middle part of the landslide mass were observed (Fig. 4a). Cracks increasingly appeared year after year from 2004 and 2006 (Fig. 4b–d).

The monitoring work of the landslide mass was started in 2007. Nine monitoring points were installed on the mass body to monitor the surface displacement by GPS, and their locations are shown in Fig. 2. Figure 5 shows the accumulative displacement of the monitored points with time. The measured displacements on block A display a stepped characteristic with time. The surface displacement suddenly increased between May and July each year, and gradually approached to a stable state in the following time.

The landslide mass had appreciable deformation in June 2009 and June 2012. This reason will be explained later. In addition, the measured results in block A were different from those in block B. Large vertical deformations were noticed by WS07-06, WS07-03, WS07-05, and WS07-02 installed

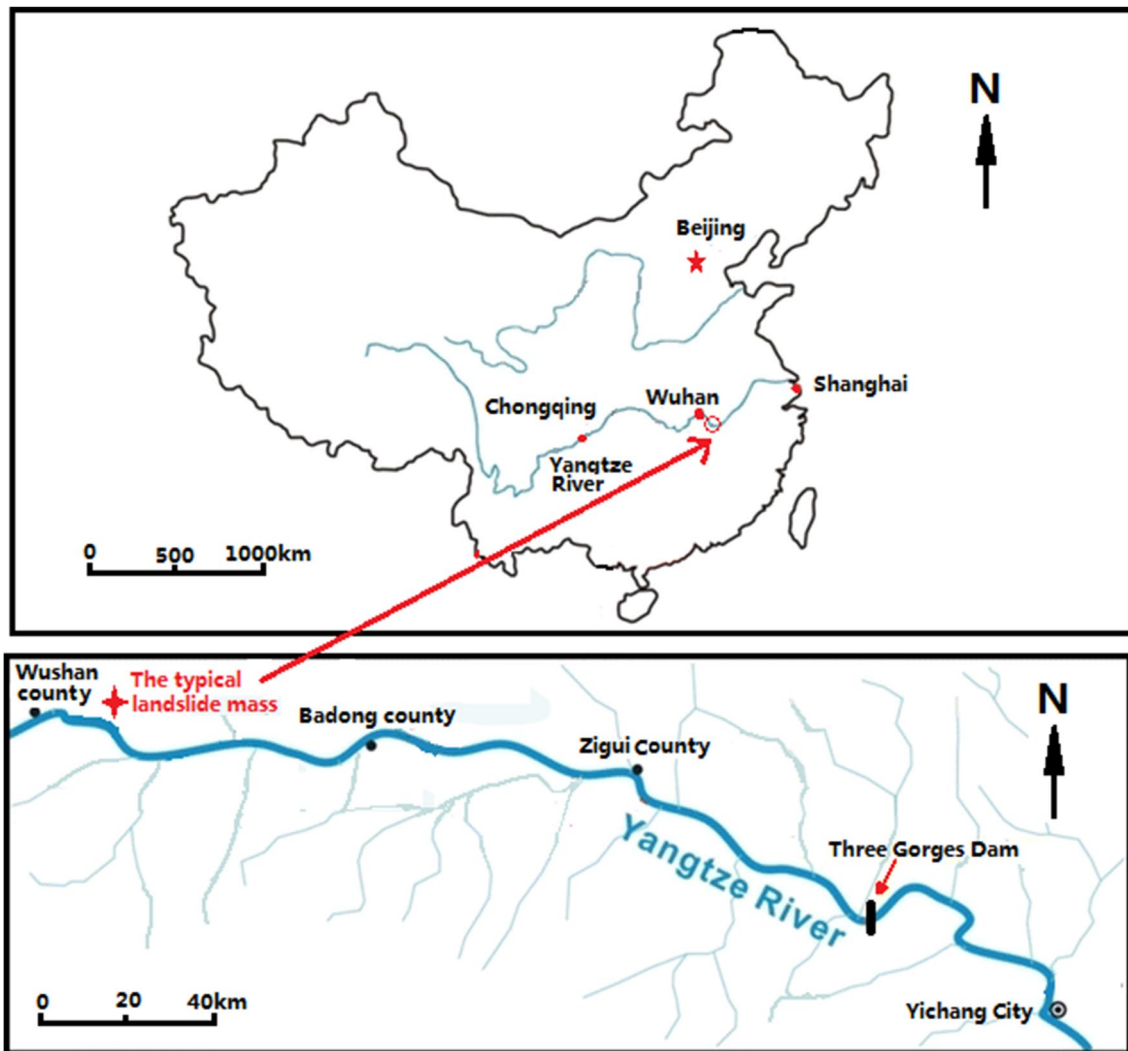


Fig. 1 Location of the landslide mass

in block A, which increased to a range of 835–994 mm. The deformations along the front edge (WS07-06, WS07-03) were greater than those of the middle part of landslide mass (WS07-05, WS07-02). The landslide mass deformed along direction angel between 147° and 155° , which was consistent with the slope direction. However, relatively small deformations by the monitored points in block B were noticed, with maximum accumulative surface displacement less than 324 mm. The deformation of the landslide mass in block B is therefore defined as trail-type deformation.

Figure 5 shows the relationship between the surface accumulative displacement of the landslide mass and the fluctuation of the water level in the TGR. The surface displacement sharply increased when the water level of the TGR dropped rapidly or was relatively low. However, the surface displacement kept relatively constant when

the water level of the TGR rose or was relatively high. It is clear that the deformation of the landslide mass was highly dependent on the water level change: it increased during the drawdown of the water level and almost kept constant during the rise of the water level.

Figure 6 shows the relationship between the deformation rate of the landslide mass and the rate of change of the water level of the TGR.

The maximal drawdown rate of water level in the reservoir reached 0.31 m/day and 0.41 m/day in 2009 and 2012, respectively, which were the top two rates among all. Meanwhile, the surface displacement had a sharper increase in 2009 and 2012 during the monitoring period. This observation further confirmed that the drawdown rate of the reservoir water level plays a significant role on the deformation of the landslide mass.

Fig. 2 Map showing the landslide mass used as typical of the research area

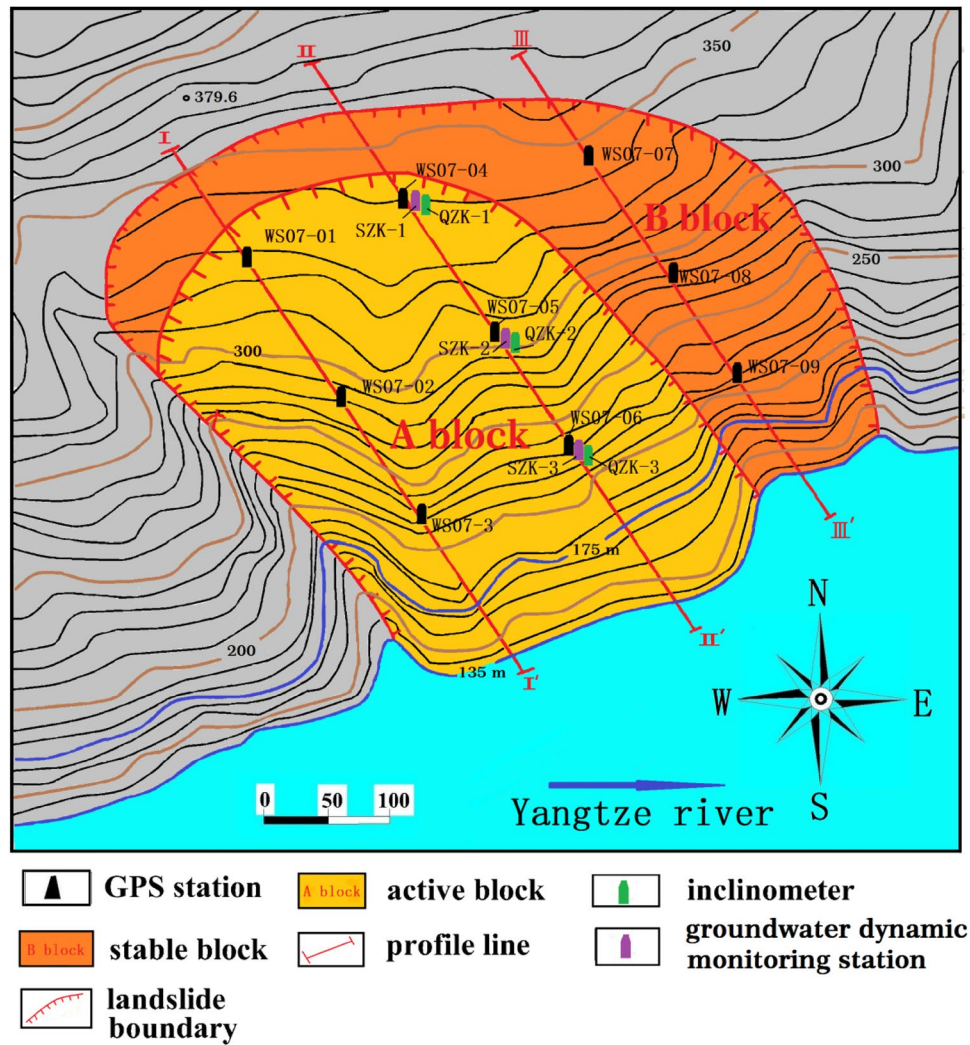


Fig. 3 Section along the II–II' profile of the typical landslide mass

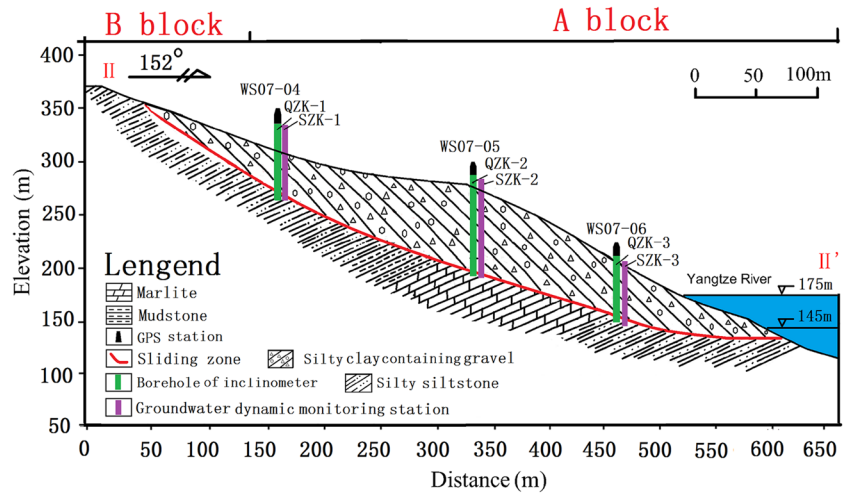


Fig. 4 Images of surface deformation phenomena

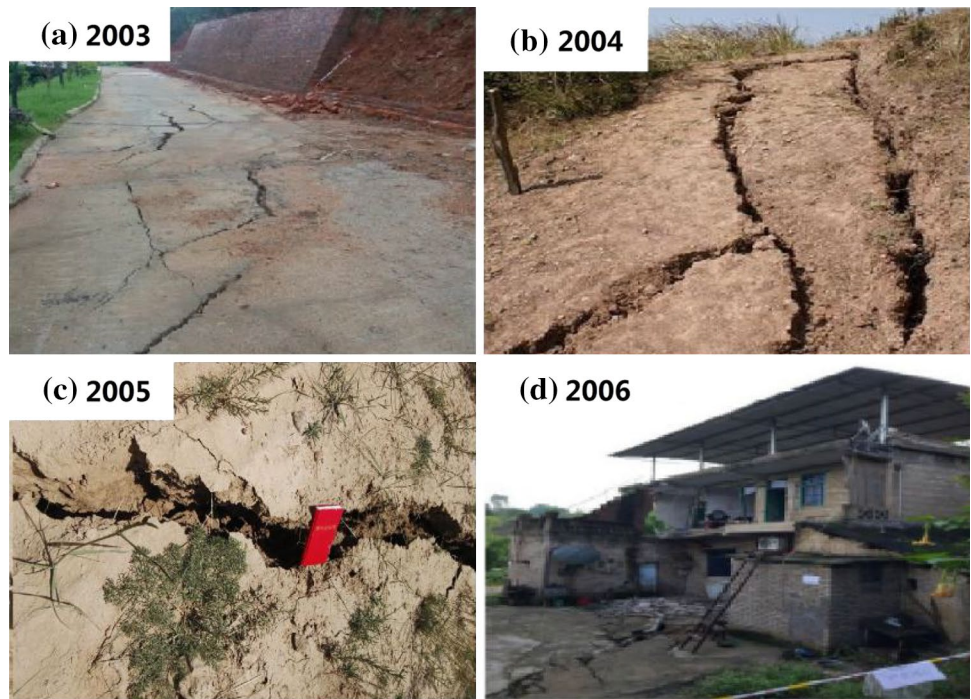
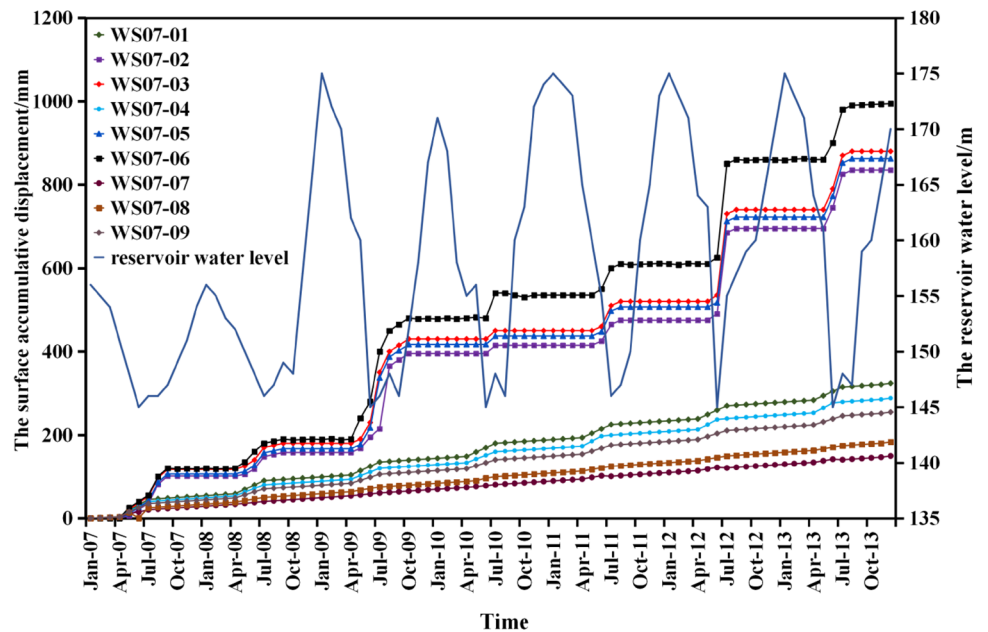


Fig. 5 Relationship between surface accumulative displacement and the reservoir water level with time



Internal lateral displacement

Three inclinometer casings (QZK-1, QZK-2, QZK-3) were installed along the profile II–II' to monitor the internal lateral displacement of the landslide mass. Figure 2 also presents the locations of the installed inclinometer casings.

QZK-1 was located on the trailing edge of the landslide mass, QZK-2 in the middle, and QZK-3 on the front edge.

Figure 7 shows the profiles of the lateral displacements at times. The influence depths of lateral displacement were 35, 70, and 60 m in QZK-1, QZK-2, and QZK-3, respectively. The surface displacement increments from

Fig. 6 Relationship between the surface accumulative displacement rate and the rate of change of reservoir water level

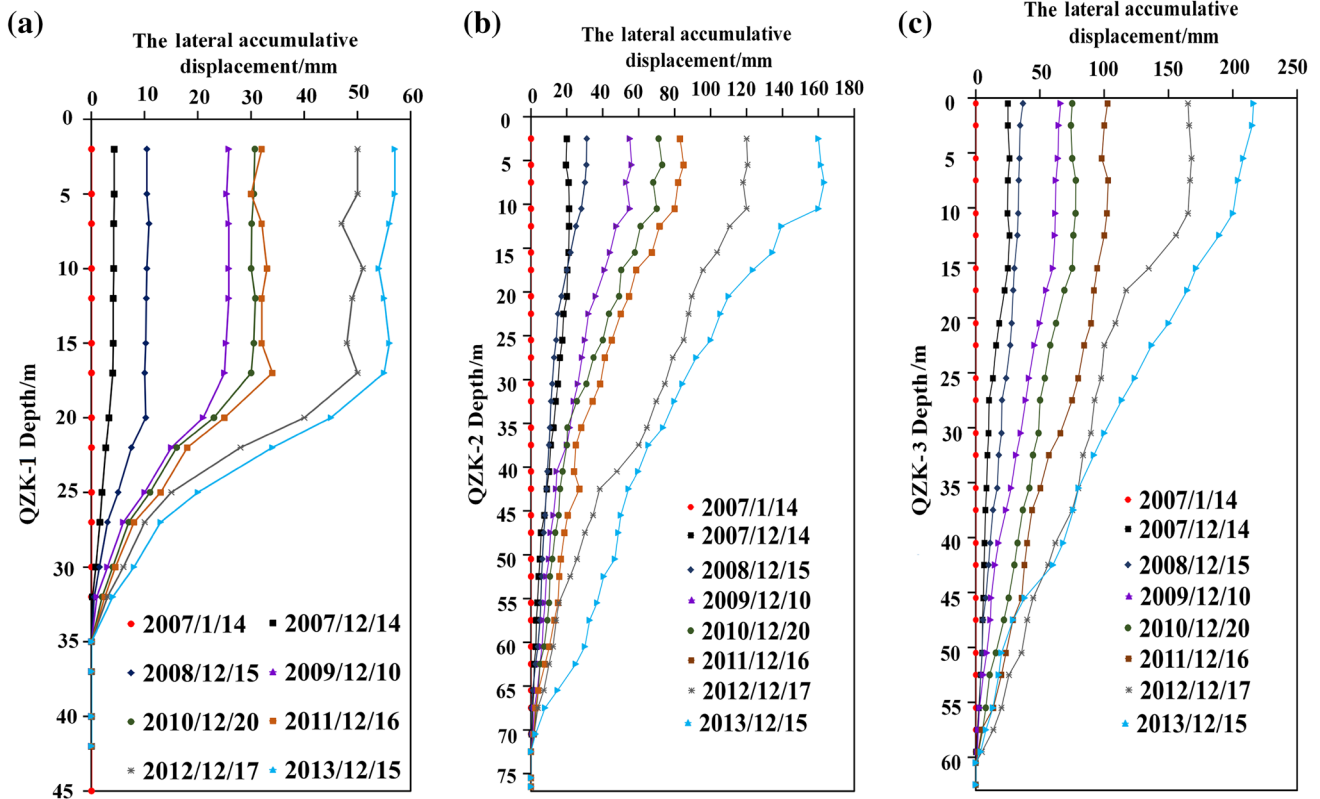
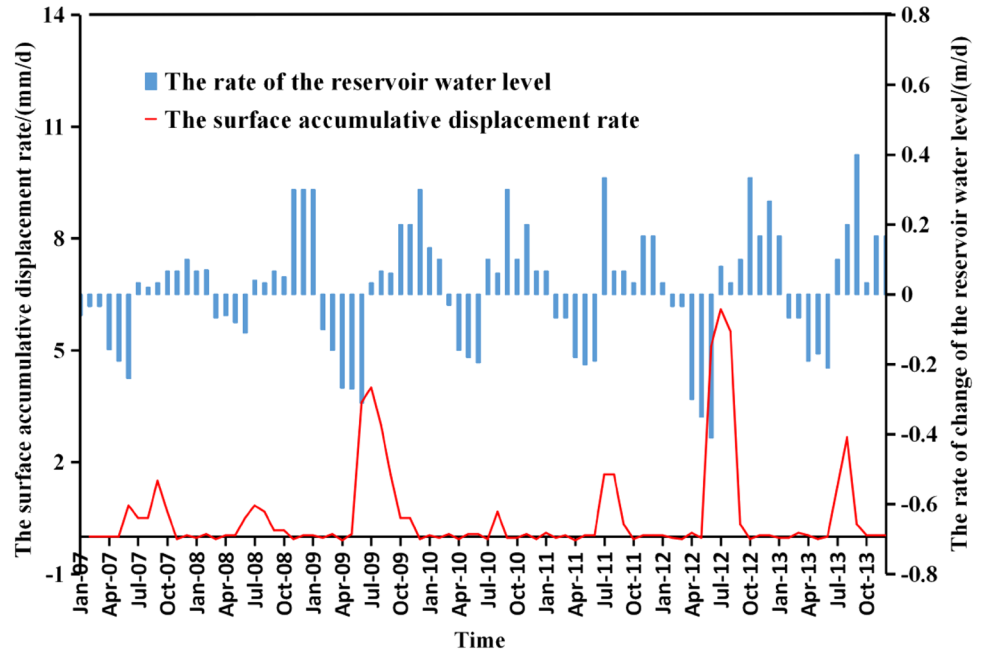


Fig. 7 Relationship between internal accumulative displacement and depth in boreholes

2007 to 2013 were 57, 161, and 216 mm in QZK-1, QZK-2, and QZK-3, respectively. The profiles of the lateral displacement in the middle part and the front edge were larger than that in the trailing edge. The lateral

displacement developed with a relative small rate from 2007 to 2011, but significantly increased in the following times. It is indicated the motion of the landslide was featured by trail mode.

Flu-solid coupling-based 3-D numerical analysis

Model establishment

Flu-solid coupling-based 3-D numerical model of the landslide was established using FLAC^{3D} to further investigate the influence of water level change on stability of landslide. Figure 8 shows the meshes of the 3-D numerical model. The 3-D geological model was first established using the ANSYS software, and then used in the FLAC^{3D} software. The geological model consisted of 343,829 grid points and 71,627 elements. The bottom boundary was fixed in all three directions (i.e., *x*, *y*, and *z* directions) and the fourth side boundary was only allowed to have in-plane displacement.

In the flu-solid coupling analysis, the rock-soil mass was regarded as porous medium and the fluid flow in pore medium satisfied both the Fourier–Biot equation and Darcy’s law. During analysis, the seepage program module was used first to generate seepage field, and then the stress field program module was used to generate the initial in situ stress field. The obtained seepage field and initial in situ stress field were combined to carry out flu-solid coupling analysis. After the interactive iteration of two modules, the stress

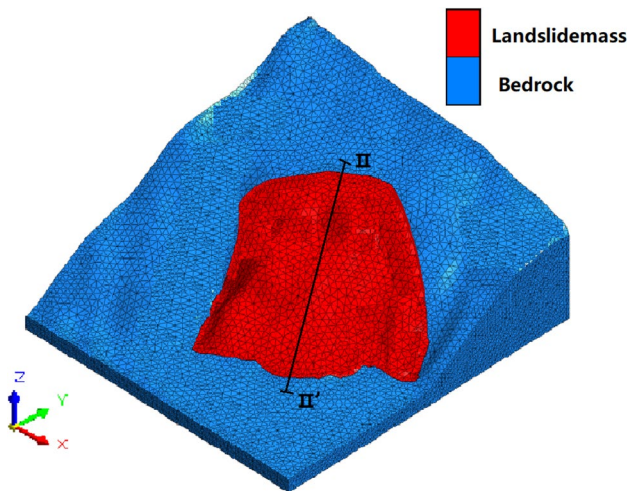


Fig. 8 3D numerical calculation model of landslide mass region

field and the seepage field were obtained under double-field convergence.

The profile II-II’ consisting of three lateral displacement profiles ZK-1, ZK-2, and ZK-3 was built to track development of the internal deformation in the landslide mass. The selected profiles had the same positions with the profile II–II’ and the inclinometer casings QZK-1, QZK-2, and QZK-3 in Fig. 2.

Material parameters

In the numerical analysis, the bedrock and the landslide mass were modeled as linearly elastic to perfectly plastic materials with the Mohr–Coulomb failure criteria. The contact zone between the landslide mass and the bedrock was modeled using strain softening model, in which the strength reduces to residual strength after reaching peak strength. Table 1 lists the material parameters used in the numerical model. The parameters of the landslide mass were determined from the laboratory and field tests. The contact surface between the slip zone and the bedrock was set as an impermeable boundary and the seepage in the bedrock was not considered (Fig. 9).

Model validation

As shown in Fig. 10, the groundwater level of the groundwater level monitoring hole SZK1 at the trailing edge of the landslide fluctuates between 255.36 and 255.83 m when the reservoir water level drops from 175 to 145 m, which is less affected by fluctuations of reservoir water level. So, it is established that the groundwater level height 255.5 m at SZK1’s position is set to the constant head boundary in the numerical model.

When the initial reservoir water level of the model is 135 m, the initial seepage field is obtained by the boundary conditions set by the model, as shown in Fig. 11. As shown in Table 2, the calculative height of the groundwater level in the seepage field is basically consistent with the actual height of the groundwater level of on-site monitoring by comparing the groundwater level of the seepage field of the groundwater monitoring holes SZK1, SZK2, and SZK3 calculated by the numerical simulation to the actual

Table 1 Numerical calculation parameters

Materials	Unit weight (kN/m ³)	Elastic modulus (GPa)	Poisson ratio	Friction angle ϕ (°)		Cohesion <i>c</i> (MPa)		Penetration coefficient (m ² /Pa s)	Porosity
				Natural state	Saturated state	Natural state	Saturated state		
Landslide mass	22.7	0.85	0.29	20	17	0.2	0.11	7×10^{-11}	0.35
Contact zone	21.7	0.75	0.31	18	15	0.1	0.06	9×10^{-11}	0.40
Bedrock	27.0	4.00	0.18	40	–	2.0	–	–	–

Fig. 9 Monitoring section and position of simulated inclinometers

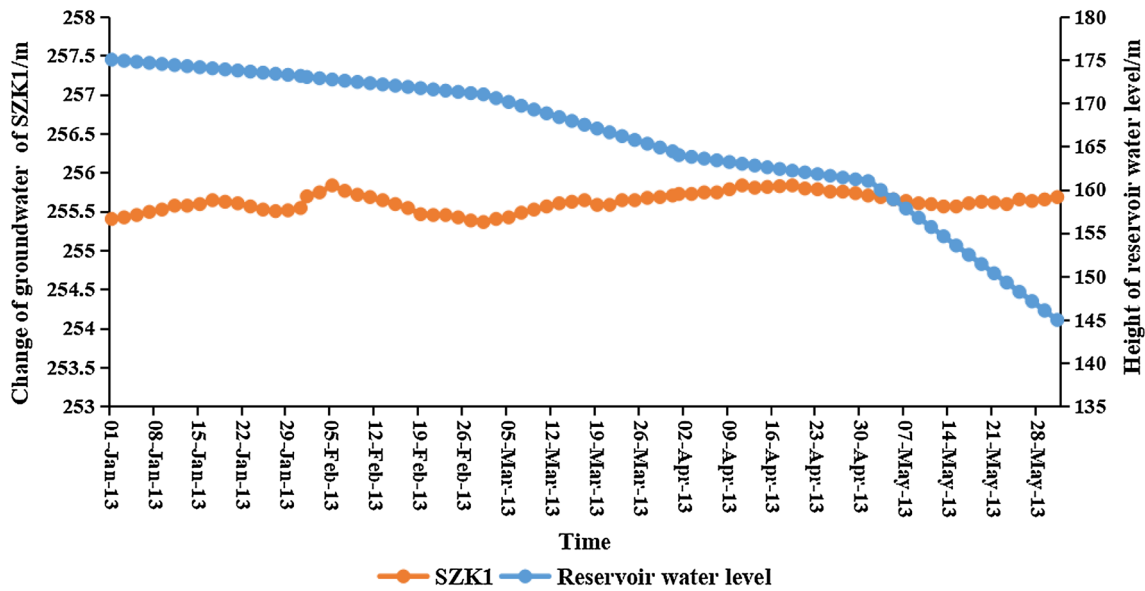
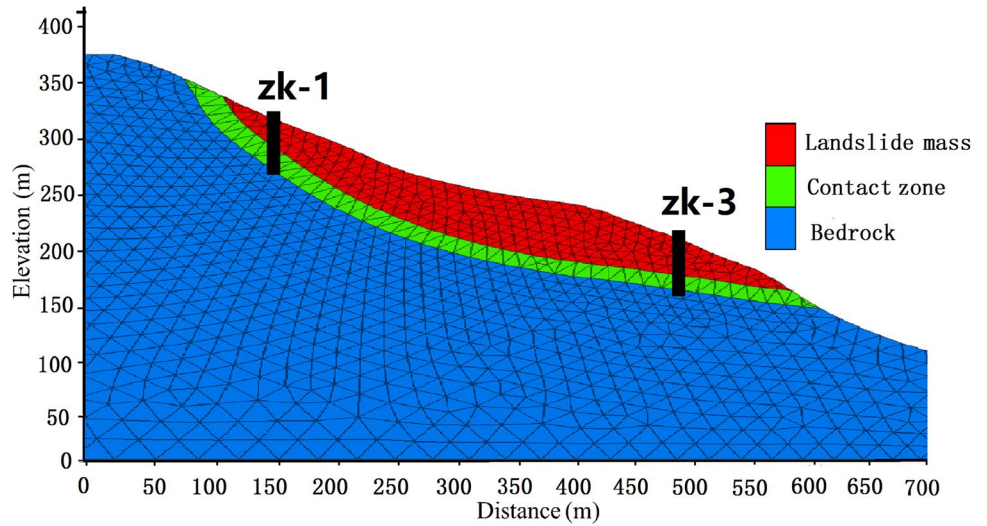


Fig. 10 The change of SZK1 groundwater level with time when the reservoir water level drops from 175 to 145 m

Fig. 11 Distribution map of groundwater seepage field when the water level of the reservoir is 135 m

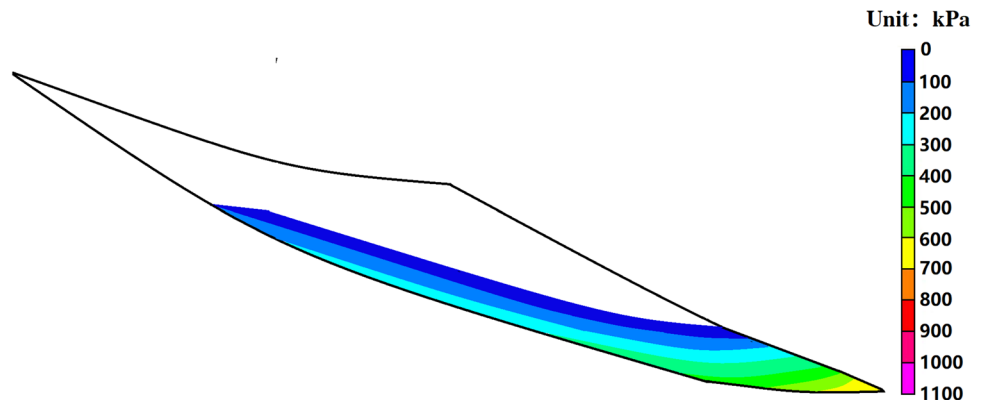


Table 2 Comparison of the actual height of the groundwater level of on-site monitoring and the calculative height of the groundwater level in the seepage field of groundwater level monitoring holes SZK1, SZK2, and SZK3 at the water level of 135 m

The on-site groundwater monitoring hole	The actual height of the groundwater level of on-site monitoring when the reservoir water level is 135 m/m	The calculative height of the groundwater level in the seepage field when the reservoir water level is 135 m/m
SZK1	255.50	255.50
SZK2	203.56	203.52
SZK3	171.21	171.23

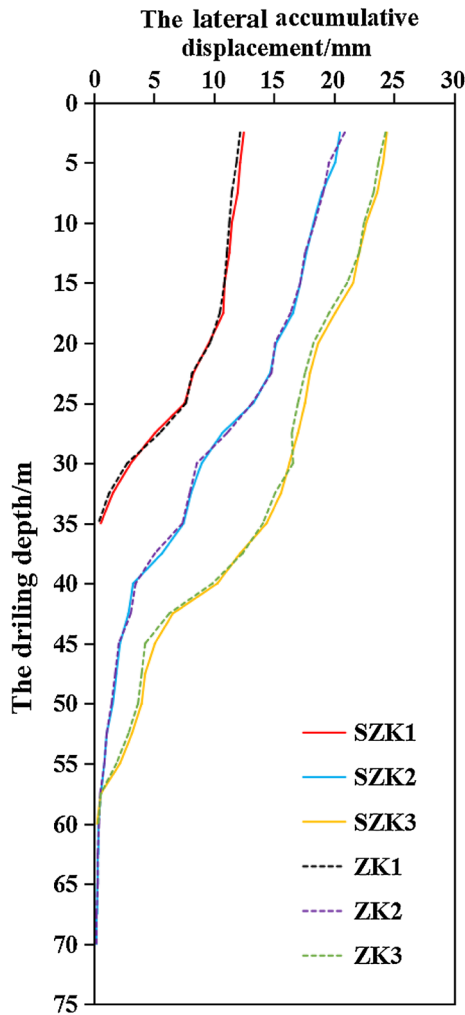


Fig. 12 Comparison of the lateral cumulative displacement increments of SZK1, SZK2, and SZK3 and the lateral cumulative displacement of ZK1, ZK2, and ZK3

groundwater level monitoring data of the three boreholes at the reservoir water level of 135 m.

Figure 12 shows that the lateral cumulative displacement increments of SZK1, SZK2, and SZK3 when the actual reservoir water level drops from 175 to 145 m from January to June 2009 are coincident nearly to the lateral cumulative displacement of ZK1, ZK2, and ZK3 when the reservoir

water level drops from 175 to 145 m and the influence depths of lateral displacement is basically same.

Numerical results and analysis

After the TGR was complete, the water level changed from 145 m and back and forth to a terminal level of 175 m. In order to investigate the influence of water level change in the reservoir on the stability of landslide mass, four cases were considered: when the reservoir was not impounded, the water level was 135 m (labeled as Case I), and then the reservoir began to impound, increasing the water level to 145 m (labeled as Case II), after that the water level increased to 175 m with a rate of 1.0 m/day (labeled as Case III), finally the water level dropped to 145 m with a rate of 1.0 m/day (labeled as Case IV).

Plastic zone of landslide mass

Figure 13a shows the plastic zone of the landslide mass in Case I when the reservoir has not been impounded. Only small local zone generated plasticity with a factor of safety of 1.68, indicating that the entire landslide mass was stable.

Figure 13b shows the plastic zone of the landslide mass in Case II. After the water level rose by 10 m, the plastic zone was largely extended from the front edge to the middle part of landslide mass. The shear opening of the landslide mass was below the reservoir water level; the front edge of landslide mass has a declining trend, and the trailing edge is in tension during the initial impoundment of the reservoir (water level of 145 m). Rising water level during the initial impoundment made the rock-soil mass that immersed into the water softened, especially of the contact zone. As a result, the strength of the landslide mass in the front edge reduced, leading to the landslide mass moving to an unstable state with the factor of safety reducing to 1.23. In reality, the rising water level enlarged the free face of the landslide mass as the front edge was easily washed out by water after it was saturated. In addition, the impoundment of the reservoir reduced the weight of the landslide mass below the water level because of buoyancy, which reduced the weight resistance against slope failure in the front edge.

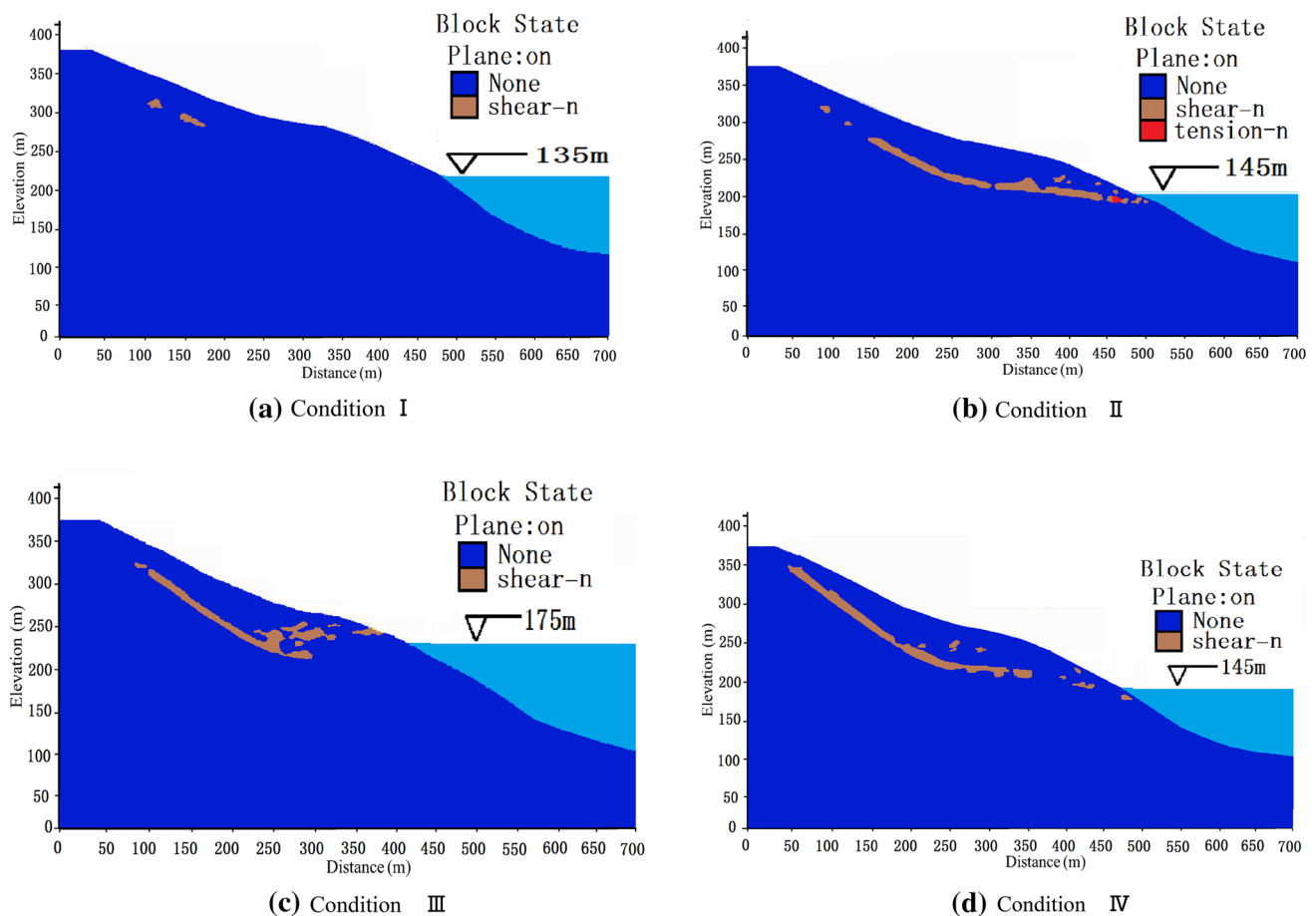


Fig. 13 Distribution of the plastic zone of a landslide mass at the different reservoir levels

Figure 13c shows the plastic zone of the landslide mass after the water level rose to 175 m (i.e., Case III). The plastic zone was further developed towards the trailing edge. The plastic zone in the front edge developed in Case III disappeared, but the landslide mass in the middle part, which was below the water level, generated some plastic zone. A change that mainly results from the level of groundwater rising as the water level rises which leads to further softening of the middle part of landslide mass and the sliding zone. The sliding of the front edge of landslide mass is obstructed due to the large hydrostatic pressure produced by the rise of the TGR water level pressing into the bottom of the landslide mass, which results in the plastic zone of the landslide mass being mainly concentrated in the middle part and the trailing edge of the landslide mass.

It can be seen that further rises of water level are adverse to the stability of the trailing edge of the landslide but favorable to the stability of the front edge of the landslide mass, and have little effect on the overall stability of the landslide mass. After the TGR was impounded to its maximum water level of 175 m, the trailing edge and the middle

part of the landslide might have been locally unstable, and the front edge of the landslide mass relatively stable.

Overall, the stability of the landslide mass had limited change when the water level rose to 175 m as the factor of safety changed from 1.28 in Case III to 1.30.

Figure 13d shows the plastic zone of the landslide mass in Case IV after the water level sank rapidly to 145 m. There was an almost complete plastic zone passing through the landslide mass.

The change is mainly resulted from the decline of the groundwater level line lags behind the drawdown of the water level, the hydrostatic pressure in the middle part of the landslide mass disappears, which leads the directions of the excess pore water pressures and the penetration forces inside of the landslide to point outward of landslide mass, the generation of the trailing force pointing outside of landslide mass is very unfavorable to the stability of the landslide mass. So, the sudden drawdown of the TGR water level will obviously destabilize the landslide mass, causing the factor of safety of the landslide mass to reach a critical value, and finally leading to a catastrophic failure of the whole landslide mass (Fig. 14).

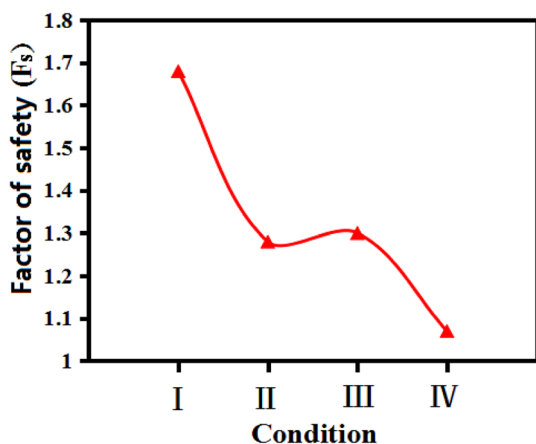


Fig. 14 Variation of the factor of safety under the different conditions

Lateral displacement

Figure 15 shows the lateral displacement profiles of ZK-1, ZK-2, and ZK-3 of Cases III and IV. The water level fluctuation had a significant influence on lateral displacement of the landslide mass. When the water level rose to 175 m, the total lateral displacement at ZK-1 was larger than that at ZK-2 and ZK-3 even though the magnitudes were small, indicating that the trailing edge slid more significantly than the front edge. Appreciable lateral displacement occurred and the lateral displacement at ZK-3 exceeded that at ZK-1 and ZK-2 with the water level dropping to 145 m, which means that the front edge slid more significantly than the trailing edge. It can also be seen that the sharp variation of lateral displacement of ZK-1, ZK-2, and ZK-3 happened near the depth of 35, 70, and 60 m, respectively, which is consistent with the position of plastic zone shown in Fig. 13d. The factor of safety of 1.07 indicates that the landslide mass closely reached its limit state under this condition.

From the above analysis, it is evidently shown that the water level change, whether up or down, had a significant reduction of stability of the landslide mass, especially the sudden drawdown. Given the current position of the reservoir and field observations, a sudden change in water level shall be strictly managed.

Landslide mode

To explore how the sliding mode varies with changes in the TGR water level, we have analyzed the displacement contours in the X-direction of the landslide under the four conditions (Fig. 16). It can be seen that the deformation of the landslide mass is mainly concentrated in the trailing edge of the landslide mass, the tension destruction is the main failure mode, and there is a transitive developmental characteristic of the push-type landslide that deforms from the

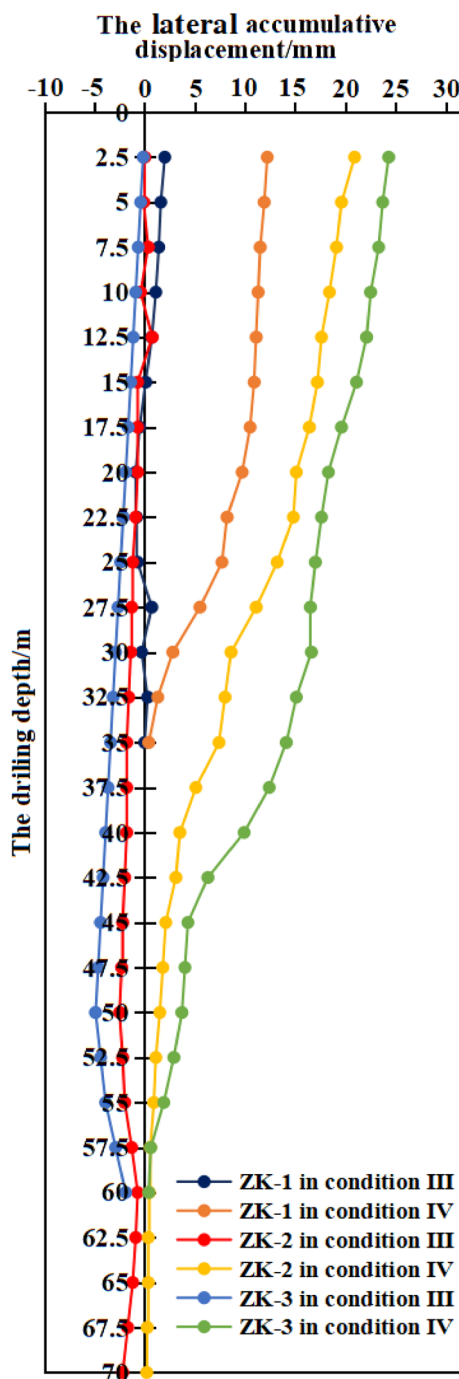


Fig. 15 The increase of the internal accumulative displacement of the simulated inclinometers

trailing edge to the front edge in condition I. The deformation of landslide mass shifts from the trailing edge to the front edge and the sliding mode shifts from the push-type landslide to the trail-type landslide because the front edge of landslide mass is influenced by the softening, and the suspension and weight loss, effects of water after impoundment (conditions II, III, and IV). It can be seen that the front part

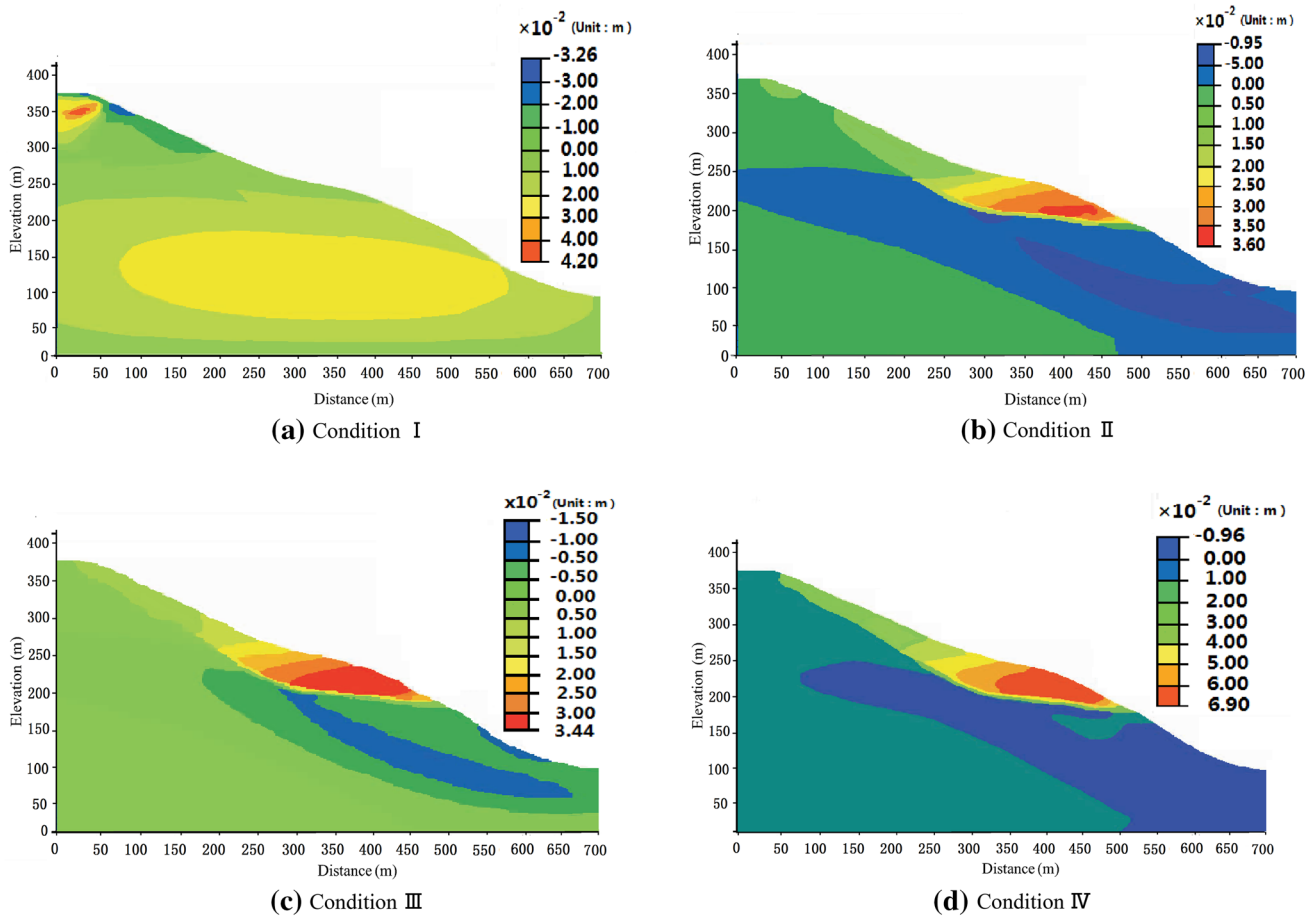


Fig. 16 The X-direction displacement contour before and after the impoundment

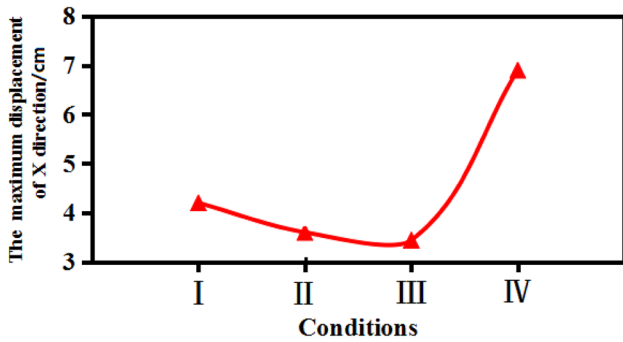


Fig. 17 The X-direction maximum displacement under the four conditions

of the landslide mass will be key to overall stability after the impoundment of the TGR region and should be considered in the process of monitoring and managing landslide risks.

Through analysis of the variation of the X-direction maximum displacement of the landslide mass (Fig. 17), we can conclude the following about the maximum displacement: first, displacement is 4.20 cm and the deformation is located along the trailing edge of the landslide if the reservoir is not

impounded (condition I); second, displacement is 3.60 cm, as the water level rises to 145 m (condition II); third, displacement is 3.44 cm (condition III) and has a low angle of declination of 4.4% compared with condition II, which is consistent with the increase of factors of safety from condition II to condition III shown in Fig. 14. Furthermore, we deduce that the sliding of the front edge of landslide mass is obstructed due to the large hydrostatic pressure produced by the rise of the TGR water level pressing into the bottom of the landslide mass. The X-direction maximum displacement of the landslide mass suddenly declines to reach 6.90 cm as the reservoir water level changes from 175 to 145 m (condition IV), which is an increase of just over 100% compared with condition II, which is consistent with the changes in the factors of safety between condition II and condition III shown in Fig. 14. The trailing force generated towards the outside of the landslide mass is generated by the forces created from excess pore water pressure and penetration.

We conclude that the impoundment of reservoir water has a significant impact on the sliding mode of a landslide: a landslide usually belongs to the push type before impoundment but then becomes a trail type after impoundment

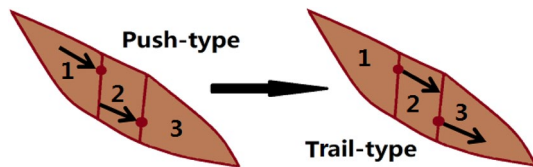


Fig. 18 Variation of sliding modes of landslides with impoundment of the TGR

(Fig. 18). Our observations here further add to our previous conclusion that a sudden drawdown of water level in the reservoir has a much greater impact upon the stability of a landslide mass than a rise of water level.

Discussion

The internal causes of deformation of any landslide mass will be due to the nature of the particular terrain, the stratigraphic lithology, and the geological structure of the landslide mass.

There is a possibility of producing a landslide if there is a slope. The landslide mass in our study is situated on a slope of the left bank of Yangtze River. Its front and trailing edges are steep, its middle part is gradual, and the average slope angle is about 25° . The planar shape of the landslide mass approximates to a square, the left and right sides of which are bounded by gullies, the trailing edge by a steep wall, all of which indicate that the free surface conditions of the slope is good. These terrain conditions are conducive to the formation and development of a landslide mass.

The occurrence of a landslide is mainly controlled by ‘slippery’ strata, such as layered strata containing planes of weakness and weak intercalation zones. In the TGR, landslide masses develop within the strata of the Badong Formation that are considered to be among the ‘easiest sliding strata’ in China (which means that landslides occur most frequently in these strata) due to their special geological setting and low strength (Fig. 3). The weak strata in the landslide region are the basic reason for the occurrence of deformation and failure of landslide masses in the region. Weak intercalation in the lower part of the landslide mass causes creep deformation under the force of gravity, which pulls the upper rock–soil mass, generating tensile deformation and gradually leading to large-scale sliding deformation.

In addition, numerous cracks have developed due to the influence of the regional geography, providing a cut surface for the formation of a landslide mass. The fact that there is a gently inclined structural plane inclined towards the outside of the landslide mass creates ideal conditions for a bottom sliding surface. In summary, these geological factors control the formation and development of landslides.

The fluctuation of reservoir water level causes the seepage field inside the bank slope to change significantly, which leads to changes in the stability of the bank slope. According to field survey data, the landslide that is the subject of our study continued to deform from 2007 to 2013, with surface cracks appearing in many places. The monitoring data of surface displacement showed that the deformation of the landslide increased sharply when water levels in the TGR declined rapidly, while the deformation was relatively small when the water level of the reservoir rose. We have verified using a $FLAC^{3D}$ numerical calculation that the rise of reservoir water level had little impact on the stability of the landslide, while the decline of reservoir water destabilized the landslide. The impact of drawdown of reservoir water level on landslide stability is greater than that of reservoir water level rise.

The fluctuation of reservoir water level causes adverse changes in the physical and mechanical properties of the rock–soil mass within the landslide; the water content of the mass changes with the rise and drawdown of the reservoir water level, which changes the structure of the mass and causes imbalances within its soil particles, water molecules, and ions, leading to decrease in strength and increase of compressibility of the mass. The rapid rise of reservoir water level has a number of effects: it increases the submerged area of the landslide, it reduces the effective stress on the sliding surface and the strength of the sliding zone, it causes the bonding force and friction coefficient between particles in the landslide to decrease, and it weakens the stability of the landslide. Rapid rise and drawdown of the reservoir water level will bring adverse changes to the seepage field in the landslide; the seepage of groundwater causes dissolution and filtration within the landslide, and causes the physical and mechanical properties of the rock–soil mass to change adversely.

When the fast drawdown of the TGR water level, the lower the TGR water level, the higher the groundwater head above the landslide. Thus, the groundwater head component along the failure surface of the landslide is counterbalanced only by attrition. The fact that the groundwater level remains practically stable proves that the hydraulic conductivity of the landslide toe is very low, and its drainage is insignificant. The groundwater of the landslide lags behind the reservoir water level. Because the groundwater infiltrates the land surface, and the water level inside the landslide remains high during drawdown of the reservoir water level, which leads to the formation of excess pore water pressure. The groundwater of the landslide mass is then discharged towards the outside of the landslide mass, generating seepage pressure points to the outside of the mass. During rapid drawdown of the reservoir water level, in addition to the osmotic pressure acting towards the outside of the sliding body, higher hydrodynamic pressure will also arise, which acts upon the soil particles, creating further instability within landslide.

Conclusions

1. Based on field monitoring data, the typical landslide mass has a stepped characteristic that reflects the change of the TGR water level. Deformation is significantly increased in the flood season, and is slow in the non-flood season. The drawdown of the reservoir water level is key to the stability of the landslide mass. There is a tendency for whole motion above the sliding zone of the landslide mass and internal deformation of the middle part and the front edge of landslide mass is strong.
2. Following analysis of the results of the numerical simulation, we have discussed the plastic zone distribution, the factors of safety and the *X*-direction maximum displacement of the landslide under four different conditions. The stability of the landslide mass is most at risk when the TGR water level varies between 175 and 145 m.
3. The sliding mode of a landslide will change from the push type to the trail type due to the effects of different hydrological environments and engineering geological conditions after the impoundment of the TGR. The dynamic water pressure generated by the drawdown of TGR water is the main reason for deformation of the landslide mass.

Acknowledgements This research is supported by the Fundamental Research Funds for the Central Universities [No. 2015XKMS035] and the Priority Academic Program Development of Jiangsu Higher Education Institutions [PAPD].

References

- Bovis MJ (1990) Rock slope deformation at affliction creek, southern Coast Mountains, British Columbia. *Can J Earth Sci* 27:243–254
- Bao YD, Han XD, Chen JP, Zhang W, Zhan JW, Sun XH, Chen M (2019) Numerical assessment of failure potential of a large mine waste dump in Panzhihua City, China. *Eng Geol* 253:171–183
- Chai C, Yu ZM, Shen ZL, Song XX, Cao XH, Yao Y (2009) Nutrient characteristics in the Yangtze River Estuary and the adjacent East China Sea before and after impoundment of the Three Gorges Dam. *Sci Total Environ* 407:4687–4695
- Chelli A, Mandrone G, Truffelli G (2006) Field investigations and monitoring as tools for modelling the Rossena castle landslide (Northern Apennines, Italy). *Landslides* 3(3):252–259
- Chen W, Yan XS, Zhao Z, Hong HY, Bui TD, Pradhan B (2019) Spatial prediction of landslide susceptibility using data mining-based kernel logistic regression, naive Bayes and RBF Network models for the Long County area (China). *Bull Eng Geol Environ* 78(1):247–266
- Deng QL, Zhu ZY, Cui ZQ, Wang XP (2000) Mass rock creep and landsliding on the Huangtupo slope in the reservoir area of the Three Gorges Project, Yangtze River, China. *Eng Geol* 58:67–83
- Du J, Yin K, Lacasse S (2013) Displacement prediction in coluvial landslides, Three Gorges Reservoir, China. *Landslide* 10(2):203–218
- Fredlund DG, Rahardjo H (1993) Soil mechanics for un-saturated soils. Wiley, New York
- He KQ, Li XR, Yan XQ (2008) The landslides in the Three Gorges Reservoir Region, China and the effects of water storage and rain on their stability. *Environ Geol* 55(1):55–63
- Huang B, Yin Y, Liu G (2012) Analysis of waves generated by Gongjiafang landslide in Wu Gorge, Three Gorges Reservoir, on November 23, 2008. *Landslides* 9:395–405
- Itasca Consulting Group, Inc (2005) FLAC 3D (fast Lagrangian analysis of continua in 3 dimensions) user manuals (version 3.0). Minneapolis, Minnesota
- Keefer DK, Wilson RC, Mark RK (1987) Real-time landslide warning during heavy rainfall. *Science* 238:921–925
- Luo XQ, Wang FW, Zhang ZH, Che AL (2009) Establishing a monitoring network for an impoundment-induced landslide in Three Gorges Reservoir Area, China. *Landslides* 6:27–37
- Matsuura S, Okamoto T, Asano S, Matsuyama K (2013) Characteristics of meltwater and/or rainfall regime in a snowy region and its effect on sediment-related disasters. *Bull Eng Geol Environ* 72:119–129
- Mayoraz F, Vulliet L (2002) Neural networks for slope movement prediction. *Int J Geomech* 2:153–173
- Nguyen TS, Likitlersuang S, Ohtsu H, Kitapka T (2017) Influence of the spatial variability of shear strength parameters on rainfall induced landslides: a case study of sandstone slope in Japan. *Arab J Geosci* 10(16):369
- Petley DN, Bulmer MH, Murphy W (2002) Patterns of movement in rotational and translational landslides. *Geology* 30:719–722
- Picarelli L, Urciuoli S, Russo C (2000) Mechanics of slope deformation and failure in stiff clays and clay shales as a consequence of pore pressure fluctuation. In: Proceedings 8th international symposium on landslides, Cardiff, vol 4, p 34
- Sassa K, Luciano P, Yin YP (2009) Monitoring, prediction and early warning. In: 1st world landslide forum, November 18–21, 2008 United Nations University, Tokyo, Japan. *Landslides Disaster Risk Reduction*, pp 351–375
- Singh TN, Singh R, Singh B, Sharma LK, Singh R, Ansari MK (2016) Investigations and stability analyses of Malin village landslide of Pune district, Maharashtra, India. *Nat Hazards* 81(3):2019–2030
- Tinti S, Bortolucci E, Armigliato A (1999) Numerical simulation of the landslide-induced tsunami of 1988 on Vulcano Island, Italy. *Bull Volcanol* 61(1–2):121–137
- Wang F, Zhang Y, Huo Z, Peng X, Araiba K, Wang G (2008) Movement of the Shuping landslide in the first four years after the initial impoundment of the Three Gorges Dam Reservoir China. *Landslides* 5(3):321–329
- Xu CC, Sun Q, Yang XY (2018) A study of the factors influencing the occurrence of landslides in the Wushan area. *Environ Earth Sci* 77:406
- Yin Y, Peng X (2007) Failure mechanism on Qianjiangping landslide in the Three Gorges Reservoir region. *Hydrogeol Eng Geol* 3:51–54
- Yu SY (2019) Numerical analysis of the seepage characteristics of slopes with weak interlayers under different rainfall levels. *Appl Ecol Environ Res* 17(5):12465–12478
- Zaniboni F, Tinti S (2014) Numerical simulations of the 1963 Vajont landslide, Italy: application of 1D Lagrangian modelling. *Nat Hazards* 70(1):567–592
- Zhang T, Yan E, Cheng J, Zheng Y (2010) Mechanism of reservoir water in the deformation of Hefeng landslide. *J Earth Sci* 6:870–875
- Zhang YG, Zhu SY, Zhang WQ, Liu Hui (2019) Analysis of deformation characteristics and stability mechanisms of typical landslide mass based on the field monitoring in the Three Gorges Reservoir, China. *J Earth Syst Sci* 128(1):9

Publisher's Note Springer Nature remains neutral with regard to jurisdictional claims in published maps and institutional affiliations.